

Pore Structure Characterization of Coal by Synchrotron Small-Angle X-ray Scattering and Transmission Electron Microscopy

Yixin Zhao,^{*,†,‡} Shimin Liu,[‡] Derek Elsworth,[‡] Yaodong Jiang,[†] and Jie Zhu[†]

[†]State Key Laboratory of Coal Resources and Safe Mining, China University of Mining and Technology, Beijing 100083, People's Republic of China

[‡]Department of Energy and Mineral Engineering, Center for Geomechanics, Geofluids, and Geohazards (G3), and Earth and Mineral Sciences (EMS) Energy Institute, Pennsylvania State University, University Park, Pennsylvania 16802, United States

ABSTRACT: Coal is a porous medium with complex pore structures. The characteristics of the pore structure play an important role in various aspects of coal use, including extraction of methane from coal seams, CO₂ sequestration in coal, and water purification by activated carbon. To describe comprehensively the pore structure of coal, we apply transmission electron microscopy (TEM) and synchrotron small-angle X-ray scattering (SAXS) measurements to six coal samples from medium to high rank. The positive deviation of SAXS data from Porod's law was observed. The positive deviation correction of SAXS data was carried out to quantitatively obtain the pore size distribution and specific surface area. We find that the pore size distribution is independent of the coal rank but varies with the vitrinite content; pores in vitrinite-rich coals are smaller than those in vitrinite-poor coals for the same rank. Channel-like and interconnected pores are observed for both high- and low-volatile bituminous coals. Among all coal samples, the low-volatile bituminous coal has the largest specific internal surface area, indicating the highest gas storage capacity and a favorable role as the best candidate for coalbed methane exploration and coal CO₂ sequestration.

1. INTRODUCTION

Coal is a naturally occurring carbon-rich porous and fractured medium. This pore structure and its characterization have an important influence on the use of coal. Coal is known as a naturally fractured dual-porosity medium, consisting of a microporous matrix and macroporous fractures, termed cleats.¹ The International Union of Pure and Applied Chemistry (IUPAC) classifies the pores into three categories in the context of physisorption: pores with widths exceeding about 50 nm are called macropores; pores of widths between 2 and 50 nm are classified as mesopores; and pores with widths less than or equal to 2 nm are called micropores.² This IUPAC pore standard is widely accepted for the characterization of coals and other types of reservoir rocks.^{3–5} The micro- and mesopores serve as reservoirs for gas storage, and the macropores provide flow pathways. Quantitative evaluation of the coal pore structure is a crucial step for the subsequent coal uses. Various methodologies have been developed to characterize the pore size distribution and total porosity of porous media. These techniques can be divided into either fluid invasion methods or radiation methods. Fluid invasion methods include both high-pressure mercury intrusion (MICP) and low-pressure adsorption (LPA) using N₂ and CO₂. Radiation methods include optical microscopy, scanning electron microscopy (SEM), transmission electron microscopy (TEM), synchrotron small-angle X-ray scattering (SAXS), small-angle neutron scattering (SANS), nuclear magnetic resonance (NMR), and X-ray micro-computed tomography (micro-CT),^{3,5,6} with more detail given in Figure 1. In this paper, pore sizes smaller than 100 nm are of principal interest. On the basis of Figure 1, TEM and SAXS are chosen to characterize the pore structure because of two reasons. The first reason is that both of them are sensitive in this pore size range, which provides us some more accurate

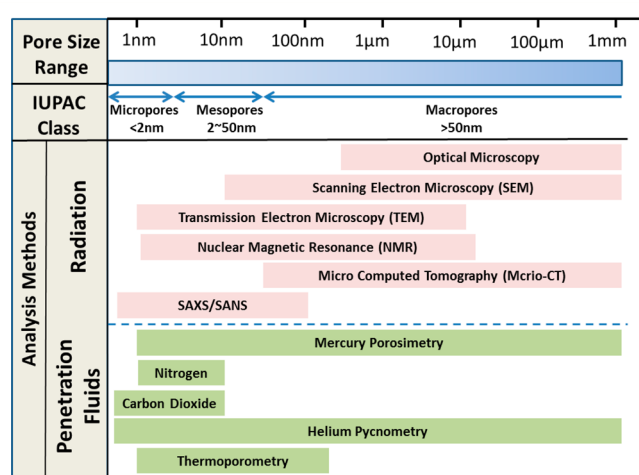


Figure 1. Methods used to estimate porosity and pore size distribution in coals or rocks. These imaging methods span six spatial orders of magnitude and include methods using both EM radiation and fluid penetration and surface sorption. This figure was modified with permission from Clarkson et al.⁶

results. Second, the interconnectedness is not a prerequisite for these two techniques, which allow us to characterize the true pore structure without the pore accessibility errors compared to the fluid invasion methods.

TEM has been historically used for the characterization of the coal structure.^{7–9} TEM uses high-energy electrons, which are accelerated close to the speed of light. The electron beam

Received: February 28, 2014

Revised: April 29, 2014

Published: April 29, 2014

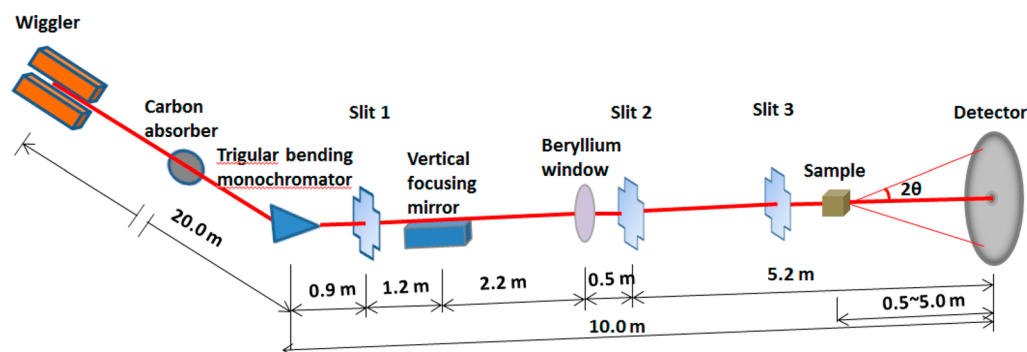


Figure 2. Diagram of beamline 1W2A and the SAXS station at BSRF. This figure was modified with permission from Li et al.³⁷

behaves as a wavefront, with a wavelength about a millions times shorter than that of visible light. When this electron beam passes through a thin-section specimen of coal, the electrons are scattered. A sophisticated system of electromagnetic (EM) focuses was used to capture the required signals, and the data were interpreted to obtain the pore structure of coal. Harris and Yust⁷ examined a high-volatile bituminous coal obtained from Perry county, eastern Kentucky, by means of TEM. The observed porosity, with exinite and inertinite constituents, falls primarily within the mesopore size range. A second series of observations on eastern Kentucky splint coal and Illinois No. 6 coal showed virinite to be micro- and mesoporous and inertinite to be mostly mesoporous.⁸ Harpalani¹⁰ observed that many micropores may not be interconnected with a corresponding impact on recoverable gas. In addition, these pores may be amorphous, granular, sponge-like, or fibrous, even within the same seam.

The SAXS technique has been historically used for coal pore structure characterization and is generally used to determine pore size distribution and specific surface area. A beam of X-rays is scattered by the electrons in an irradiated material, with the porous material providing a volume-distributed local inhomogeneity of electron density. The scattering intensity is determined mainly by the pore concentration and electron density gradient at the pore–matrix border. Among the early users, Lin et al.¹¹ reported SAXS data that indicated scattering sources in a vitrinite at sizes of 10 and 25 nm. They correlated with TEM observation of both minerals and pores in the same sample. When SAXS data were interpreted, the pore structure properties were characterized, and these properties including the radii of gyration, surface area, volume fraction, and size distributions of micropores, mesopores, and fine size minerals were all obtained. The size distributions were found to be trimodal with peaks at 3, 10, and 22 nm, with good agreement achieved between SAXS and TEM results. Bale et al.¹² reported that the macropore- and mesopore-specific surface areas obtained from SAXS data agreed with N_2 -determined surface areas of the same coals. This correlation supports the idea that N_2 adsorption at 77 K only penetrates pores of mesopore size or larger. The average pore dimension characterized by SAXS data ranged from 0.4 nm to at least 30 nm. Radliński et al.¹³ applied both SAXS and SANS techniques to determine the porosity, pore size distribution, and internal surface area of coals. Similar to Bale et al.,¹² Radliński et al.¹³ note that the results obtained by the SAXS/SANS and N_2 adsorption methods show remarkably similar trends versus vitrinite reflectance. Following this investigation, Radliński¹⁴ used both SAXS and SANS to characterize the microstructure of

sedimentary and igneous rocks, including coal. The purpose of the study was to help gain insights into internal specific surface area, porosity, pore size distribution, mercury intrusion porosimetry, and compaction. Mares et al.¹⁵ used both SAXS and SANS to investigate the microstructural properties of sub-bituminous coal from the Huntly coalfield, New Zealand. On the basis of their observations, pore size distribution and internal specific surface area were able to be measured with SAXS/ultra-small-angle X-ray scattering (USAXS) for the linear scale range from 1 to 2000 nm. Thus, the SAXS shows promise in the quantitative description of the pore structure of coal.^{3,5}

In this paper, we use SAXS and TEM techniques to examine features of the pore structure of different coals. A series of experimental investigations were executed to characterize the pore structure of six coals with various degrees of metamorphism/coalification. The positive deviation of SAXS curves from Porod's law of coals is discovered. The correction of positive deviation was then carried out. On the basis of the corrected SAXS data, the pore size distribution and specific surface area were quantitatively estimated. These results are supplemented by TEM observations. The combined SAXS and TEM investigations provide a clearer composite view of the microporosity, pore architecture, and internal surface characteristics of coals.

2. EXPERIMENTAL SECTION

2.1. Experimental Facilities. The TEM measurements were completed using a FEI Tecnai Spirit G2 electron microscope (FEI Company, Hillsboro, OR) with an associated Gatan microscopy suite that includes Digital Micrograph software for data capture and reconstruction.

The SAXS measurements reported here have been performed using synchrotron radiation as an X-ray source and a long slit collimation system at the Beijing Synchrotron Radiation Laboratory (BSRF), Beijing, China. The beamline used in this investigation is 1W2A, which is a SAXS beamline operating at a wavelength of 0.154 nm. This beamline is generated from 4-pole wiggler (1W2) at the storage ring of the Beijing electron positron collider (BEPC). A triangular bending Si (111) crystal is used to horizontally focus the beam and provide a monochromatic X-ray beam (8.052 keV).³⁵ The 1W2A beamline can be used for many conventional experimental measurements, including SAXS, wide-angle X-ray scattering (WAXS), grazing incidence SAXS (GISAXS), and time-resolved SAXS (t-SAXS). In the experiment, the recorded scattering angle (2θ) ranges from 0° to 3° and an area detector (Mar 165 CCD), set perpendicular to the incident X-rays, records the SAXS patterns.³² A schematic description of beamline 1W2A at BSRF is shown in Figure 2.

2.2. Sample Collection and Preparation. A total of six coal samples of different rank were collected from five different coal mines, all located in north China. Sample 1 was collected from the No. 9 coal seam of the Tangshan coal mine, Hebei province. Sample 2 was

Table 1. Proximate Analysis Results of Coal Samples

sample number	moisture (%)	volatile matter (%)	fixed carbon (%)	ash (%)	classification of coal ash	coal rank	sample collection
1	1.6	32.83	56.88	8.71	low ash	high-volatile A bituminous	No. 9 seam in Tangshan mine
2	1.18	9.51	60.39	14.15	medium ash	anthracite	No. 3 seam in Changzhen mine
3	0.35	7.4	84.86	7.45	low ash	anthracite	No. 2 seam in Muchengjian mine
4	2.1	34.43	57.35	5.72	low ash	high-volatile A bituminous	No. 3 seam in Muchengjian mine
5	0.57	15.6	75.99	7.88	low ash	low-volatile bituminous	No. 2 seam in Yangdong mine
6	1.56	34.54	56.67	7.89	low ash	high-volatile A bituminous	No. 11 seam in Xinzhouyao mine

obtained from the No. 3 coal seam of the Changzhen coal mine, Shanxi province. Samples 3 and 4 were acquired from the No. 2 and No. 3 seams of the Muchengjian coal mine, Beijing. Sample 5 was collected from the No. 2 coal seam of the Yangdong coal mine, Hebei province. Finally, sample 6 was obtained from the No. 11 coal seam of the Xinzhouyao coal mine, Shanxi province. All of the coal samples were carefully transported to the laboratory and then kept in an environmental chamber under controlled conditions of temperature and humidity until initiating the experiment.

For the TEM measurements, the six coal samples were argon-ion-milled. An ultrasonic drill was used to cut a rectangular sub-sample of area (2×3 mm) from each specimen with a semi-circular copper grid and then glued onto its surface. Subsequent acetone treatment was used to separate the sample from the glass substrate of the microscope slide with this composite rectangular sub-sample and then mounted into the sample holder of the ion slicer. Each sample was then thinned, so that each section of the sample was less than 100 nm in thickness. The sample preparation followed the same procedure introduced by Stojic and Brenker.¹⁶

In comparison to TEM measurements, sample preparation for the synchrotron SAXS experiment is much easier. Samples of the collected coals were crushed and sieved to obtain the appropriate particle size for the test. The pulverized coals with a particle size less than 1 mm were then used in this study.

2.3. Experimental Procedure. Prior to TEM and SAXS measurements, the coal samples were analyzed for contents of moisture, ash, volatile matter, and fixed carbon, following ASTM 2009-D5142. Petrographic composition was also defined as well as vitrinite reflectance, following standard techniques of organic petrography.¹⁷

All TEM measurements were completed at the 120 kV operating voltage, with several magnifications tuned to achieve optimal resolution of the pore structures. For the SAXS measurements, the pulverized coals filled a sample cell comprising two parallel X-ray windows sealed with 3M tape. The thickness of the sample cell was ~ 1 mm with a measurement time of ~ 4 – 10 s at a distance from the sample to the detector of 1650 mm and covering a scattering vector range of 0.1 – 3.1 nm⁻¹. The recorded SAXS two-dimensional images were processed and quantitatively converted into one-dimensional scattering data using FIT2D software.¹⁸ The original scattering data reduced by FIT2D were corrected, and the resulted data were quantitatively analyzed using Porod's law^{19,20} and a related method of deviation correction of SAXS data.²¹

3. RESULTS

3.1. Coal Sample Characterization. Proximate analysis on each sample shows that the coals are mainly of low or medium ash, with the fixed carbon content varying from 56.88 to 84.86% and moisture varying from 0.57 to 2.1%. The coal ranks include bituminous coals and anthracites, as shown in Table 1. For the bituminous coals, samples 1, 4, and 6 are high-volatile A bituminous coals and sample 5 is low-volatile bituminous coal. Samples 2 and 3 are anthracite coals.

Vitrinite reflectance measurements and maceral analyses were conducted on the polished samples of the coal samples prior to TEM analysis using a Leitz MPV-3 photometer microscope according to China National Standards GB/T 6948-1998 and GB/T 8899-1998. The selected coal samples cover a large range of thermal maturity, and the mean maximum reflectance of vitrinite $R_{o,max}$ values range from 0.81 to 6.628%, as illustrated in Table 2. The vitrinite contents range from 13.1 to 92.2%, and the inertinite contents vary from 1.6 to 81.2%, with more detailed maceral compositions included in Table 3.

Table 2. Vitrinite Reflectance Measurement Results of Coal Samples

sample number	values of vitrinite reflectance		
	R_{min} (%)	R_{max} (%)	$R_{o,max}$ (%)
1	0.908	1.129	1.115
2	3.164	4.047	4.329
3	3.268	6.691	6.628
4	0.936	1.126	1.090
5	1.349	1.455	1.454
6	0.76	0.85	0.81

3.2. TEM Results. Figure 3 shows the observed TEM images of all six samples. Coal sample 4 is highly porous and dominated with pores in the range of 10–70 nm (Figure 3d). This sample 4 is a high-volatile A coal with an extremely high vitrinite content of up to 92.2%. Although samples 1 and 6 are of the same rank as sample 4, the pore size of these two coals is much smaller than that of sample 4, as shown in panels a and f of Figure 3. This is attributed to the lower vitrinite contents of 61.6% for sample 1 and 75.4% for sample 6. Sample 5 is a low-volatile bituminous coal, which falls between high-volatile bituminous and anthracite in terms of coal rank, with a vitrinite reflectance ($R_{o,max}$) of 1.454%. Apparent from Figure 3e, sample 5 has both relatively large and channel-like pores. The channel-like pores separate the coal into slabs at the scale of observation. For the two anthracites, the pore structures of samples 2 and 3 display significantly different features. As shown in Figure 3b, the pores in sample 2 are spatially distributed and fall into the mesopore size range, with a uniform size of ~ 20 nm. Conversely, the pores in sample 3 are smaller in size, with the majority smaller than 20 nm and reaching the micropore range (< 2 nm), as shown in Figure 3c. If we compare the total vitrinite contents for these two coals, sample 2 has a much higher total of vitrinite macerals (67.8%) compared to sample 3, with only 13.1%.

Table 3. Maceral Compositions of Coal Samples

	sample number	1	2	3	4	5	6
vitrinite group	desmocollinite	35.5	41.7	6.1	17.9	66.2	19.5
	telocollinite	16.4	17.7	2.5	39.2	10.2	11.0
	telinite	4.8	4.9	4.3	32.7	1.6	41.2
	corpoeollinite	3.5	2.9		2.0	6.1	3.7
	vitrodetrinite	1.4	0.6	0.2	0.4		
inertinite group	semifusinite	6.0	16.5	38.4	0.4		10.2
	fusinite	5.2	3.9	35.9	1.0	0.2	5.3
	inertodetrinite	7.3	4.1	6.9	2.6	1.4	4.3
	macrinite						0.2
	micrinite	0.4					
liptinite group	sclerotinite	0.4					
	sporinite	1.0			0.8		1.8
	cutinite	0.2					
	resinite	0.4					
mineral matter	clay mineral	4.2	7.7	3.1	2.8	13.5	0.2
	pyrite	0.4		0.4		0.4	2.2
	carbonate mineral	12.9		2.0			0.2
	other minerals			0.2	0.2		

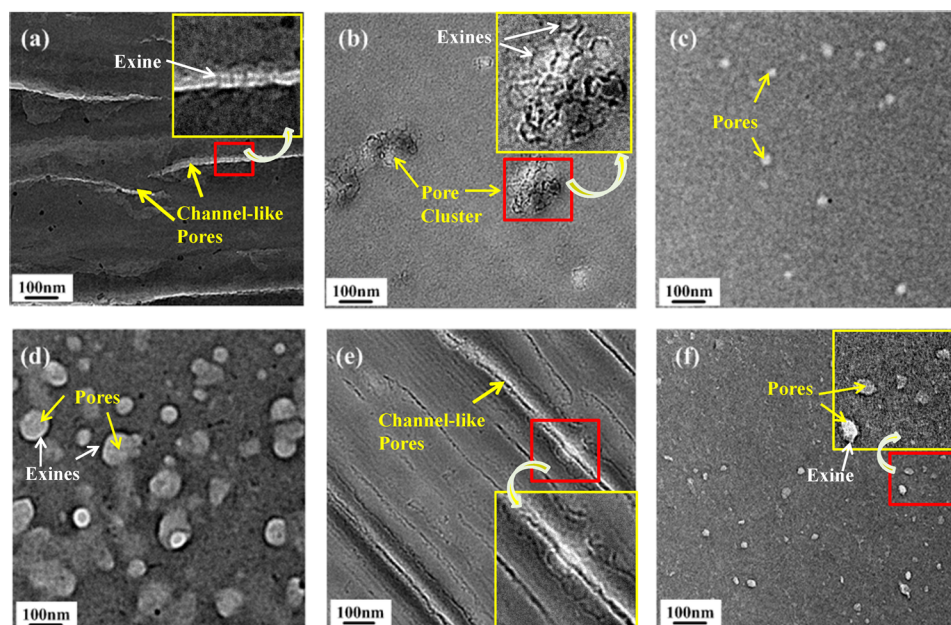


Figure 3. TEM observation results of different coal samples. Micrographs in panels a–f are typical observations of samples from 1 to 6, respectively. The enlarged yellow-bordered insets represent the red-bordered regions in the TEM images. In panels a and e, channel-like pores are observed. Some small exines can also be found in channel-like pores in panel a. Pore clusters in panel b mainly comprise mesopores of ~ 20 nm. The black exines of pores can also be observed. The pores presented in panel c are spherical pores with dim exines. The relatively larger pores and exines are more clearly shown in panel d. Panel f presents pores of irregular shape.

3.3. SAXS Results and Analysis. In SAXS experiments, a beam of X-rays with fixed wavelength and known intensity is incident on a highly transmitting sample under investigation, and the intensity of scattered radiation I is measured versus the scattering angle 2θ . Information pertinent to the size distribution of scattering objects can be retrieved from the scattering intensity, traditionally plotted versus the scattering vector, q : $q = 4\pi \sin \theta / \lambda$, where λ is the wavelength of the X-rays and 2θ is the angle between the incident X-ray beam and the detector measuring the scattered intensity, as shown in Figure 2.¹³ One interpretation of the scattering vector is that it is the resolution or yardstick with which the sample is observed. Moreover, the direction of q specifies the direction in the plane of the sample in which the structural information is collected.

For isotropically scattering samples, the two-dimensional scattering pattern registered by the detector is isotropic and may be azimuthally averaged to produce one-dimensional $I(q)$ curves.²³ Here, the original two-dimensional SAXS graphs were converted to corresponding scattering curves using the FIT2D software. Figure 4 shows the scattering curve of scattering intensity I versus scattering vector q . It can be found that the scattering intensity of sample 4 is the highest in the intermediate- and low- q regions and the scattering intensity of sample 3 is the highest in the high- q region. This result indicates the relatively higher microporosity in sample 3 and mesoporosity in sample 4.

It was also found that the SAXS results do not follow classic Porod's theory and show obvious positive deviation effects, as

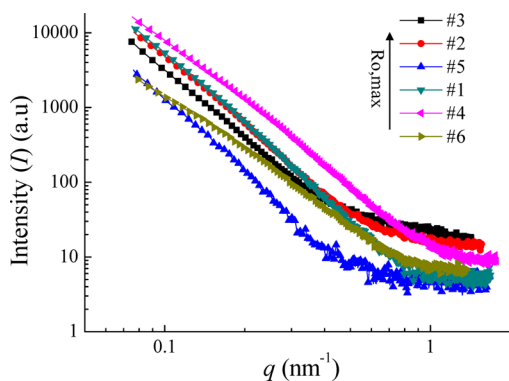


Figure 4. Scattering curves of coal samples 1–6.

shown in Figure 5. In fact, the electron density difference between the pores and the skeletons of coal is the main factor result for SAXS; the pores are main scatterers in coal. The scattering positive deviation from Porod’s law indicates that the electron density in the skeletons of coal is not uniform; i.e.,

there exist micro electron density fluctuations in the skeletons. The incomplete graphitization might be the main reason.²¹ Of course, the reasons for the positive or negative deviation upon the Porod theorem in small-angle scattering are quite complicated, and they can be influenced by many other factors, including the fluctuation of heat density of materials, small size effect of the scatterers, effects of quantum size, and surface fractal dimension, among others. However, to obtain the structure of pores in coals, the deviation should be corrected. In the present study, the analysis of pore size distribution of coal was based on the corrected SAXS data. The fundamental theory of Porod’s law deviation was explained and presented in the previous publication, and the detailed procedure of scattering data correction was also provided and validated in the publication.²¹

Figure 6 shows the log-normal distribution of the pore size for each coal sample based on methodology used by Beaucage et al.²⁴ A similar conclusion can be drawn for the TEM analysis that the pore size distribution is independent of the coal rank. Among all of the coals, the anthracite coal (sample 3) with

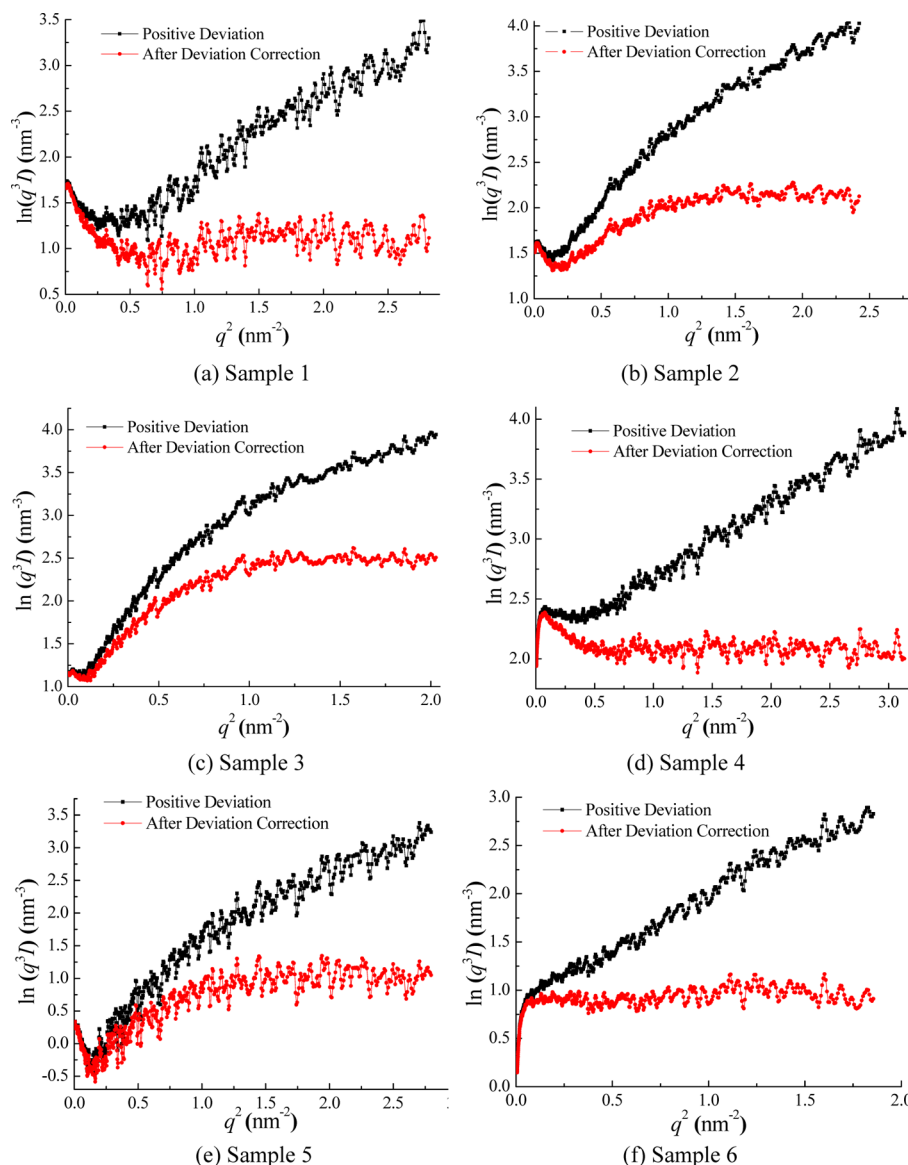


Figure 5. Porod’s curves and related deviation correction curves for the six samples.

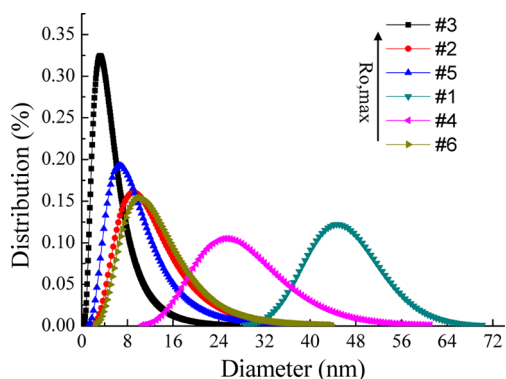


Figure 6. Resulting pore size distribution of coal samples 1–6.

$R_{o,max} = 6.628\%$ has the narrowest pore size distribution, with the pore sizes mainly falling in the window of 1–24 nm. The majority of pores distributes from 1 to 10 nm. The other anthracite coal (sample 2) with $R_{o,max} = 4.329\%$ has a relatively wider pore size distribution, varying from ~2 to ~43 nm. The low-volatile bituminous coal (sample 5) with $R_{o,max} = 1.454\%$ has a pore range from ~1 to ~38 nm, and the majority of the pore size spreads from 3 to 16 nm. For the high-volatile A bituminous coals (samples 1, 4, and 6), the pore sizes increase with the decreasing metamorphic grade of coal. The pore distributions of samples 1, 4, and 6 fall into the size windows of ~29–70, ~10–60, and ~2–44 nm. The pore size tends to decrease with an increase in the metamorphic grade if sample 5 is not taken into account.

From Figure 7, the average pore radius fluctuates with $R_{o,max}$. For the high-volatile A bituminous coals, the radius of the pore

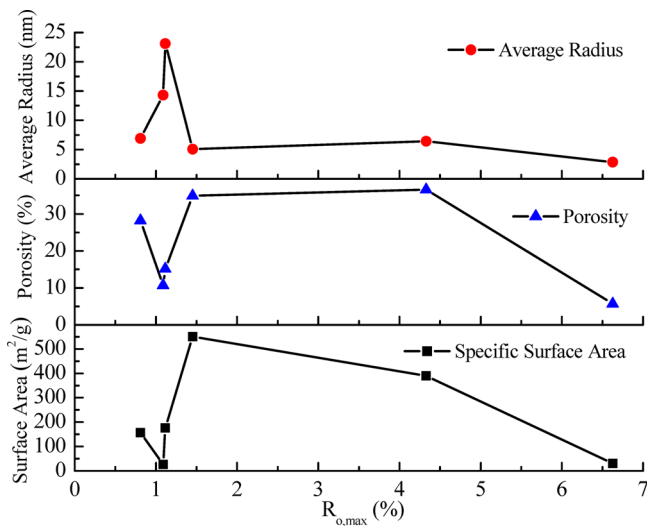


Figure 7. Relationship between the specific surface area, porosity, average radius of pores, and coal rank.

increases with the increase of $R_{o,max}$ and reaches the maximum value of 23.1 nm as $R_{o,max} = 1.115\%$. This is followed by a sudden drop on the pore radius to 5.1 nm for the low-volatile bituminous coal with $R_{o,max} = 1.454\%$ (sample 5). There is a slight increase on the average pore radius to 6.4 nm when the coal rank turns to anthracite with $R_{o,max} = 4.329\%$. For the studied samples, the computed minimum average pore radius with a value of 2.9 nm is obtained for the highest rank coal with $R_{o,max} = 6.628\%$ (sample 3).

The specific surface area is usually expressed as square meters of surface per gram of coal. It is a function of the average pore radius, pore size distribution, and porosity. The average pore radius and pore size distribution were computed on the basis of the SAXS data. To calculate the specific surface area, the mercury porosimetry porosities of all six coal samples, reported in the previous publication,²⁵ were adopted. On the basis of the collected average pore radius, size distribution, and porosity data, the specific surface area is computed and given in Table 4.

Table 4. Specific Surface Area, Average Radius of Micropores, and Porosity in Coal Samples

sample number	1	2	3	4	5	6
specific surface area (m^2/g)	175.87	389.92	30.13	26.34	550.85	157.14
average radius (nm)	23.1	6.4	2.9	14.3	5.1	6.9
porosity (%)	15.17	36.58	5.70	10.71	34.90	28.25

In Figure 7, the average pore radius, specific surface area, and porosity are plotted as a function of $R_{o,max}$. The specific surface area reaches as low as 26.34 m^2/g and as high as 550.85 m^2/g . This wide range of specific surface areas indicates that sample 5 has the highest internal surface area, which can be translated to the highest gas storage capacity. Here, the authors want to point out that the mercury porosimetry may underestimate the total porosity of coal because it can only detect accessible and connected pores.²⁶ Therefore, the true specific surface areas are expected to be greater than the estimated values using mercury porosimetry porosity.

4. DISCUSSION

TEM and SAXS imaging have been applied to characterize the complex pore structures of variable coal ranks, from medium to high. The combination of these two techniques can detect and characterize pore sizes in the range from a few angstroms to ~10 μm , as described in Figure 1. The pore structure of coal is extremely difficult to characterize because of not only the complicated pore geometry but also the wide range of the size distribution. In this study, we concentrated on the characterization of small size pores at the lower end of the size distribution (<100 nm). This range of the pore sizes is of great interest for many applications of coal, including the conversion to coking coal and the production of activated carbon for water purification. On the basis of results presented in this paper, the pore size distribution is independent of the coal rank. However, vitrinite-rich coals tend to have larger sized pores compared to vitrinite-poor coals, for the same rank of coal (bituminous coals and anthracites).

On the basis of TEM observation results in section 3.2, no direct evidence shows that the size, shape, and distribution of pores in coals is coal-rank-dependent, as described by Gan et al.²² This demonstrates that the pore size, shape, and distribution may also be influenced by paleo-environmental conditions and the post-sedimentary history of coalification and metamorphism. For these six coals, the size of pores correlates with the vitrinite maceral content for the same rank of coal; higher vitrinite content coals have larger pore sizes. It is not clear whether this is a universal correlation for a larger sampling across all coal ranks. Because the observation window in the

TEM imaging is of limited size, this censoring may impact the statistical validity of the results reported here. Fortunately, SAXS observations provide an appropriate and necessary confirmation of pore structure size distribution for a much larger and undeniably more representative sample size.

Many previous analyses of the SAXS imaging data are based on the assumption that the porous solid is a two-phase (solid-void) medium.^{12,13,27–29} However, coal is undoubtedly chemically heterogeneous and contains a variety of both organic and mineral components. Thus, coal may violate this two-phase system assumption. In addition, the complex pores of coal are neither well-separated nor non-interfering. Thus, the microheterogeneity in coals and associated density fluctuations will cause additional scattering. This additional scattering will explicitly influence the scattering curve analysis. Experimentally, the positive deviation of SAXS curves from Porod's law was observed for all six tested coal samples. This observation proves that there are additional density fluctuations in the coals. Thus, the original SAXS data essentially need to be corrected to strip off the scattering deviation to achieve the true scattering results. The methodology for correcting this positive deviation has been well-established and employed to quantitatively obtain the microstructure information on other materials.^{21,30–32} This correction method does not need SAXS measurements at very high angle, and it can be accomplished using only a single SAXS experiment.^{21,33} On the basis of this fundamental understanding of positive scattering deviation, all of the original SAXS data were corrected and then the pore structure properties were quantitatively estimated. Therefore, the obtained pore structures reflect the true pore and matrix architectures without the effects of microheterogeneity and mineral inclusion.

However, it is worth noting that all current SAXS data processing methods encounter the error problems resulting from uncertainties in physical modeling as well as in the experimental measurement system.³⁵ The relative error reported in a previous publication³⁶ is not larger than $\pm 10\%$ for the pore size characterization using the SAXS system that we employed in our research.

Additionally, all of the SAXS measurements were conducted under an ambient, sorbing-gas-free condition. However, if any sorbing gases are present in the coal, then gas condensate and adsorption may form a third phase and the two-phase assumption will be violated.^{23,34} The pore characterization of coal under a sorbing gas environment will be conducted and addressed by our subsequent research.

5. CONCLUSION

The pore structures of coals across different ranks were investigated using TEM and SAXS. The positive deviation of SAXS curves from Porod's law of coals was consistently observed for all coal samples. This observation demonstrates that the pore and matrix of coal is not an ideal two-phase system. To obtain the true pore structure properties, the SAXS deviation correction is essential to eliminate the effects of microheterogeneity and mineral inclusion. On the basis of qualitative analysis of the TEM images and quantitative analysis of the corrected SAXS images, the following conclusions are made: (1) The pore size distribution is independent of the coal rank. (2) For the same rank, vitrinite-rich coals have smaller sized pores compared to vitrinite-poor coals. (3) Microheterogeneity and mineral inclusion of coal cause the SAXS positive deviation from the ideal two-phase system. (4) Among

all coal samples, the low-volatile bituminous coal (sample 5) has the largest specific internal surface area ($550.85 \text{ m}^2/\text{g}$).

AUTHOR INFORMATION

Corresponding Author

*Telephone: +86-10-62339851. E-mail: zhaoyx@cumtb.edu.cn.

Notes

The authors declare no competing financial interest.

ACKNOWLEDGMENTS

This research is financially supported by the Major State Basic Research Development Program Fund (2010CB226804), the National Natural Science Foundation of China (51174213), the New Century Excellent Talents in Ministry of Education Support Program of China (NCET-10-0775), the Fundamental Research Funds for the Central Universities, and the Fund of the China Scholarship Council. The authors especially thank the BSRF for providing the SAXS experimental facilities and Xin Wang, Zhonghua Wu, and Guang Mo for their suggestions and aid in both conducting the experiments and analyzing the data. The authors are also thankful to the constructive comments and suggestions from the Associate Editor Ryan P. Rodgers and two anonymous reviewers.

REFERENCES

- (1) van Krevelen, D. W. *Coal: Typology—Physics—Chemistry—Constitution*, 3rd ed.; Elsevier Science: Amsterdam, Netherlands, 1993.
- (2) Sing, K. S. W.; Everett, D. H.; Haul, R. A. W.; Moscou, L.; Pierotti, R. A.; Rouquerol, J.; Siemieniowska, T. Reporting physisorption data for gas/solid systems with special reference to the determination of surface area and porosity. *Pure Appl. Chem.* **1985**, *57*, 603–619.
- (3) Bustin, R.; Bustin, A.; Cui, A.; Ross, D.; Pathi, V. Impact of shale properties on pore structure and storage characteristics. *Proceedings of the SPE Shale Gas Production Conference*; Fort Worth, TX, Nov 16–18, 2008.
- (4) Clarkson, C.; Wood, J.; Burgis, S. Nanopore-structure analysis and permeability predictions for a tight gas siltstone reservoir by use of low-pressure adsorption and mercury-intrusion techniques. *SPE Reservoir Eval. Eng.* **2012**, *15*, 648–661.
- (5) Clarkson, C. R.; Solano, N.; Bustin, R. M.; Bustin, A. M. M.; Chalmers, G. R. L.; He, L.; Melnichenko, Y. B.; Radliński, A. P.; Blach, T. P. Pore structure characterization of North American shale gas reservoirs using USANS/SANS, gas adsorption, and mercury intrusion. *Fuel* **2013**, *103*, 606–616.
- (6) Clarkson, C. R.; Jensen, J. L.; Blasingame, T. A. Reservoir engineering for unconventional gas reservoirs: What do we have to consider? *Proceedings of the SPE North American Unconventional Gas Conference and Exhibition*; Woodlands, TX, June 14–16, 2011.
- (7) Harris, L. A.; Yust, C. S. Transmission electron microscope observations of porosity in coal. *Fuel* **1976**, *55*, 233–236.
- (8) Harris, L. A.; Yust, C. S. Ultrafine structure of coal determined by electron microscopy. *Prepr. Pap.—Am. Chem. Soc., Div. Fuel Chem.* **1979**, *24*, 210–217.
- (9) Harpalani, S. Potential impact of CO₂ injection of permeability of coal. *Proceedings of First International Forum on Geological Sequestration of CO₂ in Deep, Unmineable Coalseams*; Houston, TX, March 14–15, 2002.
- (10) Harpalani, S. Gas flow through stressed coal. Ph.D. Thesis, University of California, Berkeley, CA, 1985.
- (11) Lin, J. S.; Hendricks, R. W.; Harris, L. A.; Yust, C. S. Microporosity and micromineralogy of vitrinite in a bituminous coal. *J. Appl. Crystallogr.* **1978**, *11*, 621–625.
- (12) Bale, H.; Carlson, M.; Kalliat, M.; Kwak, C.; Schmidt, P. Small-angle X-ray scattering of the submicroscopic porosity of some low-rank coals. In *The Chemistry of Low-Rank Coals*; Schobert, H. H., Ed.;

American Chemical Society (ACS): Washington, D.C., 1984; ACS Symposium Series, Vol. 264, Chapter 5, pp 79–94.

(13) Radliński, A. P.; Mastalerz, M.; Hinde, A.; Hainbuchner, M.; Rauch, H.; Baron, M.; Lin, J. S.; Fan, L.; Thiyagarajan, P. Application of SAXS and SANS in evaluation of porosity, pore size distribution and surface area of coal. *Int. J. Coal Geol.* **2004**, *59*, 245–271.

(14) Radliński, A. P. Small-angle neutron scattering and the microstructure of rocks. *Rev. Mineral. Geochem.* **2006**, *63*, 363–397.

(15) Mares, T. E.; Radliński, A. P.; Moore, T. A.; Cookson, D.; Thiyagarajan, P.; Ilavsky, J.; Klepp, J. Assessing the potential for CO₂ adsorption in a subbituminous coal, Huntly coalfield, New Zealand, using small angle scattering techniques. *Int. J. Coal Geol.* **2009**, *77*, 54–68.

(16) Stojic, A.; Brenker, F. E. Argon ion slicing (ArIS) of mineral and rock samples: A novel tool to prepare large electron transparent thin films for tem use. *Proceedings of the 40th Lunar and Planetary Science Conference*; Woodlands, TX, March 23–27, 2009.

(17) Taylor, G. H.; Teichmuller, M.; Davis, A.; Diessel, C. F. K.; Littke, R.; Robert, P. *Organic Petrology*; Gebrüder Borntraeger: Berlin, Germany, 1998.

(18) Hammersley, A. P.; Svensson, S. O.; Hanfland, M.; Fitch, A. N.; Hausermann, D. Two-dimensional detector software: From real detector to idealised image or two-theta scan. *High Pressure Res.* **1996**, *14*, 235–248.

(19) Koberstein, J. T.; Morra, B.; Stein, R. S. The determination of diffuse-boundary thicknesses of polymers by small-angle X-ray scattering. *J. Appl. Crystallogr.* **1980**, *13*, 34–45.

(20) Porod, G. Die röntgenkleinwinkelstreuung von dichtgepackten kolloiden systemen—I. Teil. *Kolloid-Z.* **1951**, *124*, 83–114.

(21) Li, Z. H. A program for SAXS data processing and analysis. *Chin. Phys. C* **2013**, *37*, 108002.

(22) Gan, H.; Nandi, S. P.; Walker, P. L. Nature of the porosity in American coals. *Fuel* **1972**, *51*, 272–277.

(23) Melnichenko, Y. B.; Radliński, A. P.; Mastalerz, M.; Cheng, G.; Rupp, J. Characterization of the CO₂ fluid adsorption in coal as a function of pressure using neutron scattering techniques (SANS and USANS). *Int. J. Coal Geol.* **2009**, *77*, 69–79.

(24) Beaucage, G.; Kammler, H. K.; Pratsinis, S. E. Particle size distributions from small-angle scattering using global scattering functions. *J. Appl. Crystallogr.* **2004**, *37*, 523–535.

(25) Wang, X. Experimental study of micropore features in coal and related effects on the performance of adsorption and desorption. M.S. Thesis, China University of Mining and Technology, Beijing, China, 2012.

(26) Ross, D. J. K.; Bustin, R. M. Characterizing the shale gas resource potential of Devonian–Mississippian strata in the western Canada sedimentary basin: Application of an integrated formation evaluation. *Am. Assoc. Pet. Geol. Bull.* **2008**, *92*, 87–125.

(27) He, L.; Melnichenko, Y. B.; Mastalerz, M.; Sakurovs, R.; Radliński, A. P.; Blach, T. Pore accessibility by methane and carbon dioxide in coal as determined by neutron scattering. *Energy Fuels* **2012**, *26*, 1975–1983.

(28) Mares, T. E.; Radliński, A. P.; Moore, T. A.; Cookson, D.; Thiyagarajan, P.; Ilavsky, J.; Klepp, J. Location and distribution of inorganic material in a low ash yield, subbituminous coal. *Int. J. Coal Geol.* **2012**, *94*, 173–181.

(29) Radliński, A. P.; Busbridge, T. L.; MacA Gray, E.; Blach, T.; Cheng, G.; Melnichenko, Y. B.; Cookson, D. J.; Mastalerz, M.; Esterle, J. Dynamic micromapping of CO₂ sorption in coal. *Langmuir* **2009**, *25*, 2385–2389.

(30) Li, Z. H.; Gong, Y. J.; Pu, M.; Wu, D.; Sun, Y. H. Determination of SiO₂ colloid core size by SAXS. *J. Mater. Sci. Lett.* **2003**, *22*, 33–35.

(31) Du, X.; Wu, E. Porosity of microporous zeolites A, X and ZSM-5 studied by small angle X-ray scattering and nitrogen adsorption. *J. Phys. Chem. Solids* **2007**, *68*, 1692–1699.

(32) Liang, L.; Xu, Y.; Hou, X.; Wu, D.; Sun, Y.; Li, Z.; Wu, Z. Small-angle X-ray scattering study on the microstructure evolution of zirconia nanoparticles during calcination. *J. Solid State Chem.* **2006**, *179*, 959–967.

(33) Li, Z. H.; Gong, Y. J.; Wu, D.; Sun, Y. H.; Wang, J.; Liu, Y.; Dong, B. Z. A negative deviation from Porod's law in SAXS of organo-MSU-X. *Microporous Mesoporous Mater.* **2001**, *46*, 75–80.

(34) Radliński, A. P.; Busbridge, T. L.; Gray, E. M. A.; Blach, T. P.; Cookson, D. J. Small angle X-ray scattering mapping and kinetics study of sub-critical CO₂ sorption by two Australian coals. *Int. J. Coal Geol.* **2009**, *77*, 80–89.

(35) Zheng, Y.; Huang, S.; Wang, L. Distribution analysis of nanoparticle size by small angle X-ray scattering. *Int. J. Theor. Appl. Nanotechnol.* **2012**, *1*, 124–133.

(36) Chen, Z. J.; Wang, W.; Cai, Q.; Chen, X.; Wu, Z. H.; Li, R. P.; Che, C. Q.; Pan, W. SAXS and XRD studies on the microstructure of TiO₂ nanoparticles. *Acta Phys. Sin.* **2008**, *57*, 5793–5799.

(37) Li, Z. H.; Wu, Z. H.; Mo, G.; Xing, X.; Liu, P. A small angle X-ray scattering station at Beijing synchrotron radiation facility. *Instrum. Sci. Technol.* **2014**, *42*, 128–141.